Supplementary Information: Emergent mesoscale correlations in active solids with noisy chiral dynamics

Amir Shee,[1,*] Silke Henkes,[2,†] and Cristián Huepe[1,3,4,‡]

[1] *Northwestern Institute on Complex Systems and ESAM, Northwestern University, Evanston, IL 60208, USA*
[2] *Lorentz Institute for Theoretical Physics, LION, Leiden University, P.O. Box 9504, 2300 RA Leiden, The Netherlands*
[3] *School of Systems Science, Beijing Normal University, Beijing, People's Republic of China*
[4] *CHuepe Labs, 2713 West August Blvd #1, Chicago, IL 60622, USA*

(Dated: September 17, 2024)

CONTENTS

I. SIMULATION MOVIES

We include the following simulation videos to show the dynamics in different regimes:

1. Movie1.mp4: Velocity fields in the Mesoscopic Range Order (MRO) regime, for $\Omega = 10^{-3}$, $D_r = 10^{-2}$.
2. Movie2.mp4: Velocity fields in the Chiral Mesoscopic Range Order (CMRO) regime, for $\Omega = 10^{-2}$, $D_r = 10^{-3}$.
3. Movie3.mp4: Velocity fields in the Dynamic Disorder (DD) regime, for $\Omega = 10^{-2}$, $D_r = 5$.
4. Movie4.mp4: Velocity fields in the Chiral Disorder (CD) regime, for $\Omega = 5$, $D_r = 10^{-2}$.
5. Movie5.mp4: Velocity fields on the critical line ($D_r = \Omega$), for high values of $\Omega = D_r = 10$, exhibiting hammering state; non-monotonic behavior of the magnitudes (i.e., of the size of the velocity vectors; shown in Fig. S.1(b)).
6. Movie6.mp4: Velocity fields for high activity $v_0 = 0.1$, in the CMRO regime ($D_r = 10^{-2}$, $\Omega = 0.1$).
7. Movie7.mp4: Velocity fields for high activity $v_0 = 0.12$, in CMRO regime ($D_r = 10^{-2}$, $\Omega = 0.1$).
8. Movie8.mp4: Velocity fields in the Chiral Mesoscopic Range Order (CMRO) regime, for equal packing fractions of CW and CCW chiral active Brownian particles ($\Omega = \pm 0.1$, $D_r = 10^{-2}$).
9. Movie9.mp4: Velocity fields of binary mixtures of particles with different chirality levels, with equal packing fractions of species A and B, for $\Omega_A = 0.1$, $\Omega_B = 0.2$, and $D_r = 10^{-2}$.

* amir.shee@northwestern.edu
† shenkes@lorentz.leidenuniv.nl
‡ cristian@northwestern.edu

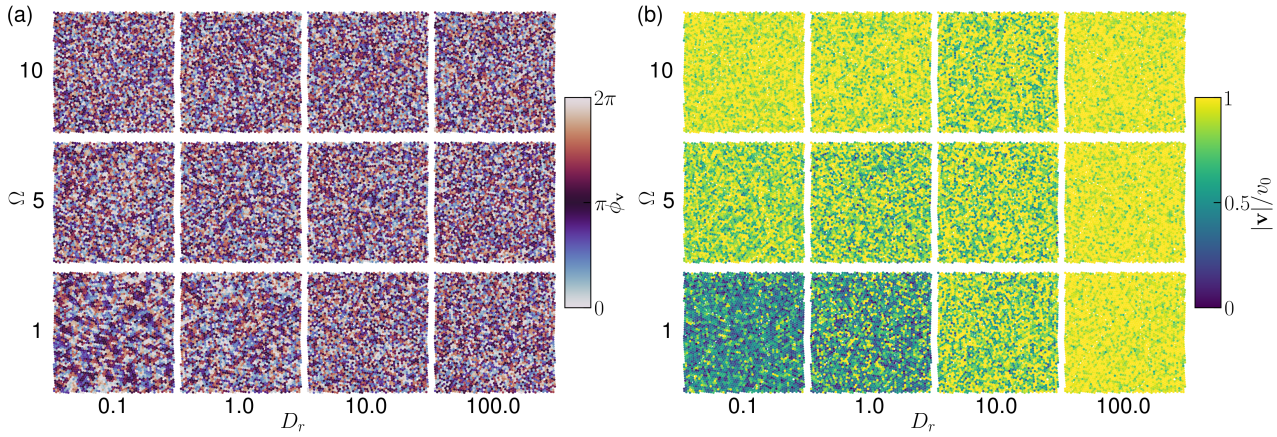

FIG. S.1. Visualization of the velocity fields for high chirality Ω and high rotational diffusion D_r values. Panel (a) show snapshots of the velocity angles $\phi_{\mathbf{v}} = \tan^{-1}(v_y/v_x)$ while panel (b) shows snapshots of the velocity amplitudes $|\mathbf{v}|/v_0 = \sqrt{v_x^2 + v_y^2}/v_0$, both in the $\Omega - D_r$ parameter space.

The active speed is set to $v_0 = 0.01$ unless stated otherwise. Other parameters include the elastic repulsion strength $k = 1$, mobility $\mu = 1$, packing fraction $\phi = 1$, and (square) system size $L = 100$, with periodic boundary conditions.

II. NORMAL MODE FORMULATION

In the absence of self-propulsion speed i.e., $v_0 = 0$, the disks have an equilibrium position $\mathbf{r}_i^0$, corresponding to a local minimum of the elastic energy. Defining small displacement around the equilibrium positions as $\delta\mathbf{r}_i = \mathbf{r}_i - \mathbf{r}_i^0$, the dynamics is described by [S1]

$$\delta\dot{\mathbf{r}}_i \;=\; v_0\hat{n}_i - \sum_j \mathbb{K}_{ij}\cdot\delta\mathbf{r}_j, \tag{S.1}$$

where the $\mathbb{K}_{ij}$'s are 2×2 blocks of the $2N\times 2N$ dynamical matrix.

We expand $\delta\mathbf{r}_i$ over the normal modes, i.e., the eigenvectors of the dynamical matrix. Each normal mode is a $2N$-dimensional vector that can be written as a list of N two-dimensional vectors $(\xi_1^\nu, ..., \xi_N^\nu)$, where $\nu = 1, ..., 2N$ labels each mode and the associated eigenvalue is denoted by λ_ν. Now, writing $\delta\mathbf{r}_i$ in the decomposed normal mode form $\delta\mathbf{r}_i = \sum_{\nu=1}^{2N} a_\nu\boldsymbol{\xi}_i^\nu$, we can project Eq. (S.1) on the normal modes, obtaining

$$\sum_{\nu=1}^{2N}\dot{a}_\nu\boldsymbol{\xi}_i^\nu \;=\; -\sum_{\nu=1}^{2N}\lambda_\nu a_\nu\boldsymbol{\xi}_i^\nu + v_0\hat{n}_i\ . \tag{S.2}$$

Taking the dot product with eigenvetors $\sum_{\nu=1}^{2N}\boldsymbol{\xi}_i^\nu$, we find

$$\sum_{\nu=1}^{2N}\dot{a}_\nu\boldsymbol{\xi}_i^\nu\cdot\sum_{\nu=1}^{2N}\boldsymbol{\xi}_i^\nu \;=\; -\sum_{\nu=1}^{2N}\lambda_\nu a_\nu\boldsymbol{\xi}_i^\nu\cdot\sum_{\nu=1}^{2N}\boldsymbol{\xi}_i^\nu + v_0\hat{n}_i\cdot\sum_{\nu=1}^{2N}\boldsymbol{\xi}_i^\nu\ ,$$

which simplifies to

$$\sum_{\nu=1}^{2N}\dot{a}_\nu\boldsymbol{\xi}_i^\nu\cdot\boldsymbol{\xi}_i^\nu \;=\; -\sum_{\nu=1}^{2N}\lambda_\nu a_\nu\boldsymbol{\xi}_i^\nu\cdot\boldsymbol{\xi}_i^\nu + v_0\hat{n}_i\cdot\sum_{\nu=1}^{2N}\boldsymbol{\xi}_i^\nu\ ,$$

Taking sum over all the particles $i = 1$ to N

$$\sum_{\nu=1}^{2N}\dot{a}_\nu\sum_{i=1}^{N}\boldsymbol{\xi}_i^\nu\cdot\boldsymbol{\xi}_i^\nu \;=\; -\sum_{\nu=1}^{2N}\lambda_\nu a_\nu\sum_{i=1}^{N}\boldsymbol{\xi}_i^\nu\cdot\boldsymbol{\xi}_i^\nu + v_0\sum_{i=1}^{N}\hat{n}_i\cdot\sum_{\nu=1}^{2N}\boldsymbol{\xi}_i^\nu\ ,$$

and considering orthonormal eigenvectors basis conditions $\sum_{i=1}^{N} \boldsymbol{\xi}_i^{\nu} \cdot \boldsymbol{\xi}_i^{\nu} = 1$, we get

$$\sum_{\nu=1}^{2N} \dot{a}_{\nu} \;=\; -\sum_{\nu=1}^{2N} \lambda_{\nu} a_{\nu} + \sum_{\nu=1}^{2N} v_0 \sum_{i=1}^{N} \hat{n}_i \cdot \boldsymbol{\xi}_i^{\nu} \;,$$

leads to the uncoupled set of equations

$$\dot{a}_{\nu} \;=\; -\lambda_{\nu} a_{\nu} + \eta_{\nu} \;, \tag{S.3}$$

corresponding to the projection of the position dynamics onto the normal modes ν. The projection of the self-propulsion force onto the normal modes ν can be written from Eq. (S.3),

$$\eta_{\nu} \;=\; v_0 \sum_{i=1}^{N} \hat{n}_i \cdot \boldsymbol{\xi}_i^{\nu} \;. \tag{S.4}$$

Now, we proceed to calculate the properties of $\eta_{\nu}(t)$. First, we compute the average of $\eta_{\nu}(t)$

$$\langle \eta_{\nu}(t) \rangle \;=\; v_0 \sum_{i=1}^{N} \langle \hat{n}_i(t) \rangle \cdot \boldsymbol{\xi}_i^{\nu} \;,$$

which leads to $\langle \eta_{\nu}(t) \rangle = 0$. Next, we calculate the two-time correlation

$$\langle \eta_{\nu}(t) \eta_{\nu'}(t') \rangle \;=\; v_0^2 \langle \sum_{i=1}^{N} \hat{n}_i(t) \cdot \boldsymbol{\xi}_i^{\nu} \sum_{i=1}^{N} \hat{n}_i(t') \cdot \boldsymbol{\xi}_i^{\nu'} \rangle \;,$$

where $\hat{n}_i$ evolves independently, which leads to

$$\langle \eta_{\nu}(t) \eta_{\nu'}(t') \rangle \;=\; v_0^2 \langle \hat{n}(t) \cdot \sum_{i=1}^{N} \boldsymbol{\xi}_i^{\nu} \hat{n}(t') \cdot \sum_{i=1}^{N} \boldsymbol{\xi}_i^{\nu'} \rangle \;.$$

Rearranging with $\hat{n}(t) \cdot \sum_{i=1}^{N} \boldsymbol{\xi}_i^{\nu} = \sum_{i=1}^{N} \boldsymbol{\xi}_i^{\nu} \cdot \hat{n}(t)$ and taking the time average of the only time dependent variable $\hat{n}(t)$, we get

$$\langle \eta_{\nu}(t) \eta_{\nu'}(t') \rangle \;=\; v_0^2 \sum_{i=1}^{N} \boldsymbol{\xi}_i^{\nu} \cdot \langle \hat{n}(t) \hat{n}(t') \rangle \cdot \sum_{i=1}^{N} \boldsymbol{\xi}_i^{\nu'} \;.$$

Expanding with $\boldsymbol{\xi}_i^{\nu} = \hat{x} \xi_i^{\nu}(x) + \hat{y} \xi_i^{\nu}(y)$ and $\hat{n} = \hat{x} n_x + \hat{y} n_y$ and setting cross terms to zero $\langle n_x n_y \rangle = \langle n_x \rangle \langle n_y \rangle = 0$, leads to

$$\langle \eta_{\nu}(t) \eta_{\nu'}(t') \rangle \;=\; v_0^2 \sum_{i=1}^{N} \langle [\xi_i^{\nu}(x) \xi_i^{\nu'}(x) n_x(t) n_x(t') + \xi_i^{\nu}(y) \xi_i^{\nu'}(y) n_y(t) n_y(t')] \rangle \;,$$

Considering the symmetry, we get

$$\langle \eta_{\nu}(t) \eta_{\nu'}(t') \rangle \;=\; \frac{v_0^2}{2} \sum_{i=1}^{N} \langle [\xi_i^{\nu}(x) \xi_i^{\nu'}(x) n_x(t) n_x(t') + \xi_i^{\nu}(x) \xi_i^{\nu'}(x) n_y(t) n_y(t') + \xi_i^{\nu}(y) \xi_i^{\nu'}(y) n_y(t) n_y(t') + \xi_i^{\nu}(y) \xi_i^{\nu'}(y) n_x(t) n_x(t')] \rangle \;,$$

$$\langle \eta_{\nu}(t) \eta_{\nu'}(t') \rangle \;=\; \frac{v_0^2}{2} \sum_{i=1}^{N} \langle [\xi_i^{\nu}(x) \xi_i^{\nu'}(x) n(t) \cdot n(t') + \xi_i^{\nu}(y) \xi_i^{\nu'}(y) n(t) \cdot n(t')] \rangle \;,$$

Rearranging again, we obtain

$$\langle \eta_{\nu}(t) \eta_{\nu'}(t') \rangle \;=\; \frac{v_0^2}{2} \langle \hat{n}(t) \cdot \hat{n}(t') \rangle \sum_{i=1}^{N} \boldsymbol{\xi}_i^{\nu} \cdot \boldsymbol{\xi}_i^{\nu'} \;,$$

Finally, using the orthonormal eigenvectors basis condition, $\sum_{i=1}^{N} \boldsymbol{\xi}_i^{\nu} \cdot \boldsymbol{\xi}_i^{\nu'} = \delta_{\nu,\nu'}$, we get

$$\langle \eta_\nu(t)\eta_{\nu'}(t')\rangle = \frac{v_0^2}{2}\langle \hat{n}(t)\cdot\hat{n}(t')\rangle \delta_{\nu,\nu'}. \tag{S.5}$$

In the absence of self-alignment, the $\theta(t)$ obey chiral-diffusive dynamics. Using the orientation autocorrelation, the final result thus becomes $\langle \eta_\nu(t)\eta_\nu(0)\rangle = (v_0^2/2)\mathrm{e}^{-D_r t}\cos\Omega t$.

From Eq. (S.3), we get

$$a_\nu(t) \;=\; a_\nu(0)\mathrm{e}^{-\lambda_\nu t} + \int_0^t dt' \eta_\nu(t')\mathrm{e}^{-\lambda_\nu(t-t')} \;. \tag{S.6}$$

The mean of $a_\nu(t)$ is $\langle a_\nu(t)\rangle = a_\nu(0)\mathrm{e}^{-\lambda_\nu t}$, in the steady-state $\langle a_\nu(t)\rangle|_{t\to\infty} = 0$. Now, we proceed to calculate $\langle a_\nu^2(t)\rangle$,

$$\langle a_\nu^2(t)\rangle \;=\; \langle a_\nu^2(0)\rangle \mathrm{e}^{-2\lambda_\nu t} + \mathrm{e}^{-2\lambda_\nu t}\int_0^t dt' \int_0^t dt'' \langle \eta_\nu(t')\eta_\nu(t'')\rangle \mathrm{e}^{\lambda_\nu(t'+t'')} \;. \tag{S.7}$$

Substituting the autocorrelation of $\eta_\nu(t)$ gives

$$\langle a_\nu^2(t)\rangle \;=\; \langle a_\nu^2(0)\rangle \mathrm{e}^{-2\lambda_\nu t} + \frac{v_0^2}{2}\mathrm{e}^{-2\lambda_\nu t}\int_0^t dt' \int_0^t dt'' \mathrm{e}^{\lambda_\nu(t'+t'')}\mathrm{e}^{-D_r|t'-t''|}\cos\left(\Omega|t'-t''|\right) \;. \tag{S.8}$$

Rewriting,

$$\langle a_\nu^2(t)\rangle \;=\; \langle a_\nu^2(0)\rangle \mathrm{e}^{-2\lambda_\nu t} + \frac{v_0^2}{2}\mathrm{e}^{-2\lambda_\nu t} I(t) \;. \tag{S.9}$$

We now proceed to calculate the integration $I(t)$, given by

$$I(t) \;=\; \int_0^t dt' \int_0^t dt'' \mathrm{e}^{\lambda_\nu(t'+t'')}\mathrm{e}^{-D_r|t'-t''|}\cos\left(\Omega|t'-t''|\right) \;. \tag{S.10}$$

We can split the above integration in two parts $I = I_1 + I_2$ based on the conditions $I_1(t)$ for $t' > t''$ and $I_2(t)$ for $t'' > t'$. Let's consider the first case $t' > t''$:

$$I_1(t) \;=\; \int_0^t dt' \int_0^{t'} dt'' \mathrm{e}^{\lambda_\nu(t'+t'')}\mathrm{e}^{-D_r(t'-t'')}\cos\left[\Omega(t'-t'')\right] \;. \tag{S.11}$$

Similarly for $t'' > t'$:

$$I_2(t) \;=\; \int_0^t dt'' \int_0^{t''} dt' \mathrm{e}^{\lambda_\nu(t'+t'')}\mathrm{e}^{-D_r(t''-t')}\cos\left[\Omega(t''-t')\right] \;. \tag{S.12}$$

Solving these integrals analytically can be quite challenging due to the exponential and cosine terms. However, we can always expand the cosine term using Euler's formula and applying to the $I_1(t)$ gives

$$I_1(t) \;=\; \frac{1}{2}\int_0^t dt' \int_0^{t'} dt'' \mathrm{e}^{\lambda_\nu(t'+t'')}\mathrm{e}^{-D_r(t'-t'')}\left(\mathrm{e}^{[i\Omega(t'-t'')]} + \mathrm{e}^{[-i\Omega(t'-t'')]}\right) \;. \tag{S.13}$$

Now, considering the symmetry of the problem, $I_1 = I_2$, and we get $I = 2I_1$

$$I(t) \;=\; \frac{(D_r+\lambda_\nu)\left(\mathrm{e}^{2\lambda_\nu t}-1\right)}{\lambda_\nu[(D_r+\lambda_\nu)^2+\Omega^2]} - \frac{\left(\mathrm{e}^{(\lambda_\nu - D_r + i\Omega)t}-1\right)}{(\lambda_\nu + D_r - i\Omega)(\lambda_\nu - D_r + i\Omega)} - \frac{\left(\mathrm{e}^{(\lambda_\nu - D_r - i\Omega)t}-1\right)}{(\lambda_\nu + D_r + i\Omega)(\lambda_\nu - D_r - i\Omega)} \;. \tag{S.14}$$

In the limit of $t\to\infty$, we calculate $\langle a_\nu^2\rangle = \lim_{t\to\infty}\langle a_\nu^2\rangle(t)$ in the steady-state

$$\langle a_\nu^2\rangle \;=\; \frac{v_0^2(D_r+\lambda_\nu)}{2\lambda_\nu\left[(D_r+\lambda_\nu)^2+\Omega^2\right]} \;. \tag{S.15}$$

The average energy per mode $E_\nu = \lambda_\nu\langle a_\nu^2\rangle/2$ in the steady-state then reads

$$E_\nu \;=\; \frac{v_0^2(D_r+\lambda_\nu)}{4\left[(D_r+\lambda_\nu)^2+\Omega^2\right]} \;. \tag{S.16}$$

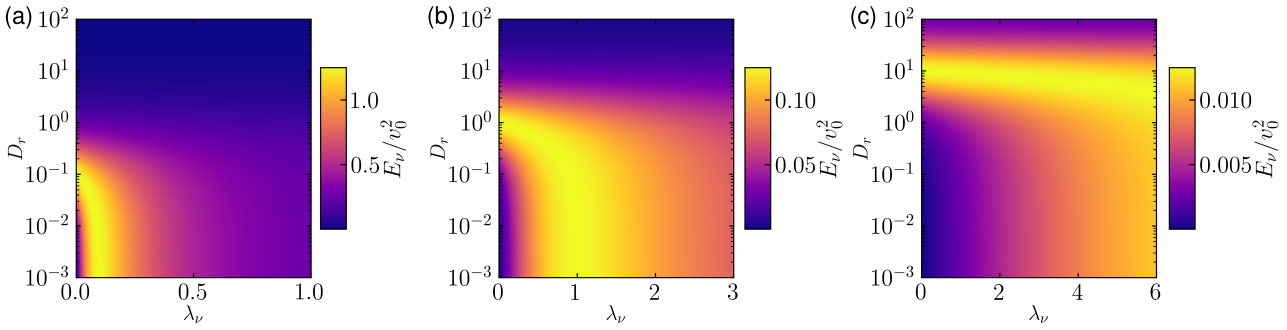

FIG. S.2. Visualization of the mean energy resulting for high chirality levels. The panels present colorplots of E_ν/v_0^2, given by Eq. (S.16), as a function of the λ_ν eigenvalues and of the rotational diffusion coefficient D_r, for fixed chirality (a) $\Omega = 0.1$, (b) $\Omega = 1$, and (c) $\Omega = 10$.

A. Spatial velocity correlations in Fourier space

We consider the velocity-velocity correlation function in Fourier space, where one can express the (discrete) Fourier transform $\mathbf{v}(\mathbf{q})$ as a function of the particles reference positions $\mathbf{r}_i^0$: $\langle|\mathbf{v}(\mathbf{q})^2|\rangle = \langle\mathbf{v}(\mathbf{q})\cdot\mathbf{v}^*(\mathbf{q})\rangle$, with $\mathbf{v}(\mathbf{q}) = \sum_{j=1}^N e^{i\mathbf{q}\cdot\mathbf{r}_j^0}\delta\dot{\mathbf{r}}_j/N$. Expanding over the normal modes, one finds $\langle|\mathbf{v}(\mathbf{q})^2|\rangle = \sum_{\nu,\nu'}\langle\dot{a}_\nu\dot{a}_{\nu'}\rangle\boldsymbol{\xi}_\nu(\mathbf{q})\cdot\boldsymbol{\xi}^*_{\nu'}(\mathbf{q})$ with $\boldsymbol{\xi}_\nu(\mathbf{q}) = \sum_{j=1}^N e^{i\mathbf{q}\cdot\mathbf{r}_j^0}\boldsymbol{\xi}_j^\nu/N$, where $\boldsymbol{\xi}_\nu(\mathbf{q})$ is the Fourier transform of the vectors $\boldsymbol{\xi}_\nu$. As, the modes are uncorrelated, we rewrite $\langle|\mathbf{v}(\mathbf{q})^2|\rangle = \sum_{\nu,\nu'}\langle\dot{a}_\nu^2\rangle|\boldsymbol{\xi}_\nu(\mathbf{q})|^2\delta_{\nu\nu'}$. Now we proceed to calculate $\langle\dot{a}_\nu^2\rangle$

$$\langle\dot{a}_\nu^2\rangle = \lambda_\nu^2\langle a_\nu^2\rangle - 2\lambda_\nu\langle a_\nu\eta_\nu\rangle + \langle\eta_\nu^2\rangle\ . \tag{S.17}$$

The first term $\langle a_\nu^2\rangle$ was already calculated in Eq. (S.15). We now calculate $\langle a_\nu\eta_\nu\rangle$. Multiplying $\eta_\nu(t)$ to the Eq. (S.6) leads to

$$\langle a_\nu\eta_\nu\rangle = a_\nu(0)e^{-\lambda_\nu t}\langle\eta_\nu(t)\rangle + \int_0^t dt'\langle\eta_\nu(t)\eta_\nu(t')\rangle e^{-\lambda_\nu(t-t')}\ . \tag{S.18}$$

The first term $\langle\eta_\nu(t)\rangle = 0$, gives

$$\langle a_\nu\eta_\nu\rangle = \int_0^t dt'\langle\eta_\nu(t)\eta_\nu(t')\rangle e^{-\lambda_\nu(t-t')}\ , \tag{S.19}$$

substituting $\langle\eta_\nu(t)\eta_\nu(t')\rangle$ produces

$$\langle a_\nu\eta_\nu\rangle = \frac{v_0^2}{2}\int_0^t dt' e^{-D_r|t-t'|}\cos\left(\Omega|t-t'|\right)e^{-\lambda_\nu(t-t')}\ , \tag{S.20}$$

with $t > t'$. Then

$$\langle a_\nu\eta_\nu\rangle = \frac{v_0^2}{2}\int_0^t dt' e^{-(D_r+\lambda_\nu)(t-t')}\cos\left(\Omega(t-t')\right)\ , \tag{S.21}$$

$$\langle a_\nu\eta_\nu\rangle = \frac{v_0^2}{4}\int_0^t dt' e^{-(D_r+\lambda_\nu)(t-t')}\left(e^{[i\Omega(t-t')]} + e^{[-i\Omega(t-t')]}\right)\ . \tag{S.22}$$

After performing a very simple integration of above equation, setting the steady-state limit $t\to\infty$ gives,

$$\langle a_\nu\eta_\nu\rangle = \frac{v_0^2(D_r+\lambda_\nu)}{2[(D_r+\lambda_\nu)^2+\Omega^2]}\ . \tag{S.23}$$

Now, the third term of Eq. (S.17) gives $\langle\eta_\nu^2\rangle = v_0^2/2$. Finally, we get the velocity correlation function $\langle|\mathbf{v}(\mathbf{q})^2|\rangle = \sum_\nu\langle\dot{a}_\nu^2\rangle|\boldsymbol{\xi}_\nu(\mathbf{q})|^2$ using Eq. (S.17), Eq. (S.15), and Eq. (S.23). This leads to

$$\langle|\mathbf{v}(\mathbf{q})^2|\rangle = \frac{v_0^2}{2}\sum_\nu\left[1 - \frac{\lambda_\nu(D_r+\lambda_\nu)}{(D_r+\lambda_\nu)^2+\Omega^2}\right]|\boldsymbol{\xi}_\nu(\mathbf{q})|^2\ , \tag{S.24}$$

where $\boldsymbol{\xi}_\nu(\mathbf{q})$ is the Fourier transform of the vector $\boldsymbol{\xi}_i^\nu$. For $\Omega = 0$, Eq. (S.24) simplifies to the velocity correlation function for active Brownian disks studied by Henkes et al. in [S1]:

$$\langle|\mathbf{v}(\mathbf{q})^2|\rangle \;=\; \frac{v_0^2}{2}\sum_\nu \frac{D_r}{D_r+\lambda_\nu}|\boldsymbol{\xi}_\nu(\mathbf{q})|^2 \;. \tag{S.25}$$

In the other limit, with $D_r = 0$, the deterministic chiral active motion gives

$$\langle|\mathbf{v}(\mathbf{q})^2|\rangle \;=\; \frac{v_0^2}{2}\sum_\nu \frac{\Omega^2}{\Omega^2+\lambda_\nu^2}|\boldsymbol{\xi}_\nu(\mathbf{q})|^2 \;. \tag{S.26}$$

III. CONTINUUM ELASTIC FORMULATION

We describe here a mathematical framework of the continuum elasticity formulation for chiral active solids, in terms of their deformation and stress distribution, in presence of active forces and constant torque.

Isotropic elastic solid: In two dimensions, the elastic energy of an isotropic elastic solid with bulk modulus B and shear modulus G can be written as [S2]

$$F_{\rm el} \;=\; \frac{1}{2}\int d^2\mathbf{r}\left[B\;\mathrm{Tr}(\hat{u}(\mathbf{r}))^2 + 2G\left(2u_{\alpha\beta}(\mathbf{r}) - \frac{1}{2}\mathrm{Tr}(\hat{u}(\mathbf{r}))\delta_{\alpha\beta}\right)^2\right] \;, \tag{S.27}$$

where $\hat{u}$ is the strain tensor with components $u_{\alpha\beta} = \frac{1}{2}\left[\partial_\alpha u_\beta + \partial_\beta u_\alpha\right]$ written as spatial derivatives of the components $\alpha, \beta \in \{x, y\}$ of the displacement vectors $\mathbf{u}(\mathbf{r}) = \mathbf{r}'(\mathbf{r}) - \mathbf{r}$ from a reference state $\mathbf{r}$ to the deformed state $\mathbf{r}'(\mathbf{r})$. The stress tensor $\sigma_{\alpha\beta} = \frac{\delta F_{\rm el}}{\delta u_{\alpha\beta}}$ can then be written as $\sigma_{\alpha\beta} = B\delta_{\alpha\beta}u_{\gamma\gamma} + 2G(u_{\alpha\beta} - \frac{1}{2}\delta_{\alpha\beta}u_{\gamma\gamma})$, where the summation over pairs of repeated indices is assumed. We can then write the overdamped equations of motion for the displacement field as $\dot{u}_\alpha = \partial_\beta\sigma_{\alpha\beta}$, in vectorial form as

$$\dot{u} \;=\; B\nabla\left(\nabla\cdot\mathbf{u}\right) + G\Delta\mathbf{u} \;. \tag{S.28}$$

In Fourier space $\tilde{\mathbf{u}}(\mathbf{q},t) = \int d^2\mathbf{r}\;\mathbf{u}(\mathbf{r},t)\mathrm{e}^{i\mathbf{q}\cdot\mathbf{r}}$ with $\mathbf{q} = (q_x, q_y)$, we can write this relation as

$$\dot{\tilde{u}} \;=\; -\mathbb{D}(\mathbf{q})\tilde{u} \;, \tag{S.29}$$

where the 2×2 dynamic matrix in Fourier space written as

$$\mathbb{D}(\mathbf{q}) \;=\; \begin{bmatrix} Bq_x^2 + Gq^2 & Bq_xq_y \\ Bq_xq_y & Bq_y^2 + Gq^2 \end{bmatrix}, \tag{S.30}$$

where $q^2 = q_x^2 + q_y^2$.

Isotropic active elastic solid: In the presence of self-propulsion force, the continuum equation of motion is given by [S1]

$$\dot{\mathbf{u}} \;=\; \nabla\cdot\sigma + \mathbf{f}_{\rm act} \;. \tag{S.31}$$

In our model, the active force is $\mathbf{f}_{\rm act}(\mathbf{r},t) = v_0\hat{n}(\mathbf{r},t)$. In order to compare our simulation results and continuum theory, the numerical computations are done for relatively large system size but finite size of L, with a minimum length scale given by the particle size $a = 2r_0$, where r_0 is the radius of the particle. This guides us to perform discrete space Fourier transformation in numerical analysis. On the other hand, by setting $L\to\infty$ and $a\to 0$ in the analytic calculation give the results in hydrodynamic limit. For consistency between two approaches, we use the following space continuous Fourier transform $\mathbf{u}(\mathbf{r},t) = \frac{1}{(2\pi)^2}\int d^2\mathbf{q}\;\tilde{\mathbf{u}}(\mathbf{q},t)\mathrm{e}^{-i\mathbf{q}\cdot\mathbf{r}}$. By considering the finite system and particle sizes, we discretize the integral into $\frac{1}{(2\pi)^2}\int d^2\mathbf{q} \to \frac{1}{Na^2}\sum_{\mathbf{q}}$ and $\int d^2\mathbf{r} \to a^2\sum_r$, where $N = 4\phi L^2/\pi a^2$, ϕ is the packing fraction of the system close to 1 for dense systems. In the sum $\mathbf{q}$ takes discrete values defined by the geometry of the problem. For instance a square lattice of linear size L, $\mathbf{q} \equiv (q_x, q_y) = 2\pi/L(m,n)$ where integers m, n satisfying $0 \le m, n \le L/a - 1$. Thus, the discrete space Fourier transform $\mathbf{u}(\mathbf{q},t)$ is related to the continuous Fourier transform $\tilde{\mathbf{u}}(\mathbf{q},t)$ through $\tilde{\mathbf{u}}(\mathbf{q},t) = a^2\mathbf{u}(\mathbf{q},t)$.

To proceed with the computations in the framework of continuum theory, we now introduce space and time Fourier transform: $\mathbf{u}(\mathbf{r},t) = \frac{1}{(2\pi)^3}\int d^2\mathbf{q}\int d\omega\;\tilde{\mathbf{u}}(\mathbf{q},\omega)\mathrm{e}^{-i(\mathbf{q}\cdot\mathbf{r}+\omega t)}$ and $\tilde{\mathbf{u}}(\mathbf{q},\omega) = \int d^2\mathbf{r}\int dt\;\mathbf{u}(\mathbf{r},t)\mathrm{e}^{i(\mathbf{q}\cdot\mathbf{r}+\omega t)}$, with these definitions, the equation of motion (S.31) can be rewritten in Fourier space as

$$-i\omega\tilde{\mathbf{u}}(\mathbf{q},\omega) \;=\; \tilde{\mathbf{f}}_{\rm act}(\mathbf{q},\omega) - \mathbb{D}(\mathbf{q})\tilde{\mathbf{u}}(\mathbf{q},\omega) \;, \tag{S.32}$$

where we have defined the continuous Fourier transform $\tilde{\mathbf{f}}_{\rm act}(\mathbf{q},\omega)$ of the active force $\mathbf{f}_{\rm act}(\mathbf{r},t)$ in Fourier space as

$$\tilde{\mathbf{f}}_{\rm act}(\mathbf{q},\omega) \;=\; v_0 \int d^2\mathbf{r} \int_{-\infty}^{\infty} dt\; \hat{n}(\mathbf{r},t)\; \mathrm{e}^{i(\mathbf{q}\cdot\mathbf{r}+\omega t)} \;. \tag{S.33}$$

Active noise correlations: To determine the correlation of active orientation, we need to start from a spatially discretized version of the model. For definiteness, we assume a square grid with lattice spacing a. Then for each grid node i we have $\hat{n}_i = (\cos(\theta_i), \sin(\theta_i))$ with dynamics presented in equation of motion Eq. (2) of the main text, which is spatially uncorrelated and we thus have $\langle \hat{n}_i(t)\cdot\hat{n}_j(t')\rangle = \delta_{i,j}\langle\hat{n}(t)\cdot\hat{n}(t')\rangle$. In order to take a continuum limit, we replace $\hat{n}_i$ by a continuous field, and we substitute $\delta_{i,j}$ by its Dirac counterpart, $\delta_{i,j}\to a^2\delta(\mathbf{r}-\mathbf{r}')$. We then have that in continuum limit $\langle\hat{n}(\mathbf{r},t)\cdot\hat{n}(\mathbf{r}',t')\rangle = a^2\delta(\mathbf{r}-\mathbf{r}')\langle\hat{n}(t)\cdot\hat{n}(t')\rangle$. In view of Eq. (S.33), it is clear that $\langle\tilde{\mathbf{f}}_{\rm act}(\mathbf{q},\omega)\rangle = 0$ and second order correlations $C_{\tilde{F}} = \langle\tilde{\mathbf{f}}_{\rm act}(\mathbf{q},\omega)\cdot\tilde{\mathbf{f}}_{\rm act}(\mathbf{q}',\omega')\rangle$ are simply

$$C_{\tilde{F}} \;=\; \frac{2(2\pi)^3 a^2 v_0^2 D_r}{(\omega-\Omega)^2+D_r^2}\delta(\mathbf{q}+\mathbf{q}')\delta(\omega+\omega') \;. \tag{S.34}$$

For finite system size L, we replace the Dirac delta by the Kronecker delta, $\delta(\mathbf{q}+\mathbf{q}')\to\frac{1}{(\Delta q)^2}\delta_{\mathbf{q}',-\mathbf{q}}$, with $\Delta q \equiv 2\pi/L$. We are thus led to define the space-discrete Fourier transform $\mathbf{f}_{\rm act}(\mathbf{q},\omega) = \tilde{\mathbf{f}}_{\rm act}(\mathbf{q},\omega)/a^2$ for discrete wave vectors $\mathbf{q}$ with continuous variable ω. The correlation of the discrete Fourier transform $\mathbf{f}_{\rm act}(\mathbf{q},\omega)$ reads $C_F = \langle\mathbf{f}_{\rm act}(\mathbf{q},\omega)\cdot\mathbf{f}_{\rm act}(\mathbf{q}',\omega')\rangle$

$$C_F \;=\; \frac{N\pi^2 v_0^2 D_r}{\phi\left[(\omega-\Omega)^2+D_r^2\right]}\delta(\omega+\omega') \;. \tag{S.35}$$

A. Spatial velocity correlation

We decompose equation (S.33) into longitudinal and transverse mode: $\tilde{\mathbf{u}} = \tilde{u}_L(\mathbf{q},\omega)\hat{\mathbf{q}} + \tilde{u}(\mathbf{q},\omega)\hat{\mathbf{q}}_\perp$ along and perpendicular to the eigenvectors of the dynamical matrix in equation (S.29). We obtain two equations,

$$-\mathrm{i}\omega\tilde{u}_{\rm L}(\mathbf{q},\omega) \;=\; \tilde{\mathbf{f}}_{\rm act}(\mathbf{q},\omega)\cdot\hat{\mathbf{q}} - (B+G)q^2\tilde{u}_{\rm L}(\mathbf{q},\omega) \;, \tag{S.36}$$

$$-\mathrm{i}\omega\tilde{u}_{\rm T}(\mathbf{q},\omega) \;=\; \tilde{\mathbf{f}}_{\rm act}(\mathbf{q},\omega)\cdot\hat{\mathbf{q}}^{\perp} - Gq^2\tilde{u}_{\rm T}(\mathbf{q},\omega) \;, \tag{S.37}$$

with solution

$$\tilde{u}_{\rm L}(\mathbf{q},\omega) \;=\; \frac{\tilde{\mathbf{f}}^{\rm L}_{\rm act}(\mathbf{q},\omega)}{-\mathrm{i}\omega+(B+G)q^2} \;, \tag{S.38}$$

$$\tilde{u}_{\rm T}(\mathbf{q},\omega) \;=\; \frac{\tilde{\mathbf{f}}^{\rm T}_{\rm act}(\mathbf{q},\omega)}{-\mathrm{i}\omega+Gq^2} \;, \tag{S.39}$$

where $\tilde{\mathbf{f}}^{\rm L}_{\rm act}(\mathbf{q},\omega) = \tilde{\mathbf{f}}_{\rm act}(\mathbf{q},\omega)\cdot\hat{\mathbf{q}}$ and $\tilde{\mathbf{f}}^{\rm T}_{\rm act}(\mathbf{q},\omega) = \tilde{\mathbf{f}}_{\rm act}(\mathbf{q},\omega)\cdot\hat{\mathbf{q}}^{\perp}$.

We can use these expressions to obtain velocity correlation functions that can be directly measured in simulations. As $\tilde{\mathbf{v}}(\mathbf{q},\omega) = -\mathrm{i}\omega\tilde{\mathbf{u}}(\mathbf{q},\omega)$, we can simply write

$$\begin{aligned}\langle\tilde{\mathbf{v}}(\mathbf{q},\omega)\cdot\tilde{\mathbf{v}}(\mathbf{q}',\omega')\rangle \;&=\; \langle\tilde{v}_{\rm L}(\mathbf{q},\omega)\tilde{v}_{\rm L}(\mathbf{q}',\omega')\rangle + \langle\tilde{v}_{\rm T}(\mathbf{q},\omega)\tilde{v}_{\rm T}(\mathbf{q}',\omega')\rangle \\ &=\; -\omega\omega'\left[\langle\tilde{u}_{\rm L}(\mathbf{q},\omega)\tilde{u}_{\rm L}(\mathbf{q}',\omega')\rangle + \langle\tilde{u}_{\rm T}(\mathbf{q},\omega)\tilde{u}_{\rm T}(\mathbf{q}',\omega')\rangle\right] \;.\end{aligned} \tag{S.40}$$

In the case of isotropic active force, it is easy to show that the longitudinal and transverse components of the active force contribute equally to the correlation,

$$\begin{aligned}\langle\tilde{\mathbf{f}}^{\rm L}_{\rm act}(\mathbf{q},\omega)\tilde{\mathbf{f}}^{\rm L}_{\rm act}(\mathbf{q}',\omega')\rangle \;&=\; \langle\tilde{\mathbf{f}}^{\rm T}_{\rm act}(\mathbf{q},\omega)\tilde{\mathbf{f}}^{\rm T}_{\rm act}(\mathbf{q}',\omega')\rangle \\ &=\; \frac{1}{2}\langle\tilde{\mathbf{f}}_{\rm act}(\mathbf{q},\omega)\tilde{\mathbf{f}}_{\rm act}(\mathbf{q}',\omega')\rangle \\ &=\; \frac{C_{\tilde{F}}}{2} \;.\end{aligned} \tag{S.41}$$

The correlation functions of longitudinal and transverse components of the Fourier velocity field are therefore

$$\langle\tilde{v}_{\rm L}(\mathbf{q},\omega)\tilde{v}_{\rm L}(\mathbf{q}',\omega')\rangle \;=\; -\omega\omega'\langle\tilde{u}_{\rm L}(\mathbf{q},\omega)\tilde{u}_{\rm L}(\mathbf{q}',\omega')\rangle \;, \tag{S.42}$$

$$\langle\tilde{v}_{\rm T}(\mathbf{q},\omega)\tilde{v}_{\rm T}(\mathbf{q}',\omega')\rangle \;=\; -\omega\omega'\langle\tilde{u}_{\rm T}(\mathbf{q},\omega)\tilde{u}_{\rm T}(\mathbf{q}',\omega')\rangle \;. \tag{S.43}$$

Utilizing Eq. (S.38) and Eq. (S.39) and substituting Eq. (S.41), we find

$$\langle \tilde{v}_{\rm L}(\mathbf{q},\omega)\tilde{v}_{\rm L}(\mathbf{q}',\omega')\rangle \;=\; \frac{\omega^2 C_{\tilde{F}}}{2\left[(B+G)^2q^4+\omega^2\right]}\;, \tag{S.44}$$

$$\langle \tilde{v}_{\rm T}(\mathbf{q},\omega)\tilde{v}_{\rm T}(\mathbf{q}',\omega')\rangle \;=\; \frac{\omega^2 C_{\tilde{F}}}{2\left[G^2q^4+\omega^2\right]}\;. \tag{S.45}$$

To calculate the equal-time Fourier transform of the velocity, we need to integrate over frequency, i.e., for spatial longitudinal velocity correlation, we obtain

$$\langle \tilde{v}_{\rm L}(\mathbf{q},t)\tilde{v}_{\rm L}(\mathbf{q}',t)\rangle \;=\; \frac{1}{(2\pi)^2}\int_{-\infty}^{\infty}d\omega\int_{-\infty}^{\infty}d\omega' \mathrm{e}^{-\mathrm{i}(\omega+\omega')t}\langle \tilde{v}_{\rm L}(\mathbf{q},\omega)\tilde{v}_{\rm L}(\mathbf{q}'\omega')\rangle\;. \tag{S.46}$$

A straightforward integration leads to

$$\langle \tilde{v}_{\rm L}(\mathbf{q},t)\tilde{v}_{\rm L}(\mathbf{q}',t)\rangle \;=\; 2\pi^2a^2v_0^2\frac{D_r((B+G)q^2+D_r)+\Omega^2}{\left((B+G)q^2+D_r\right)^2+\Omega^2}\delta(\mathbf{q}+\mathbf{q}')\;. \tag{S.47}$$

Similarly, for the spatial transverse velocity correlation we find

$$\langle \tilde{v}_{\rm T}(\mathbf{q},t)\tilde{v}_{\rm T}(\mathbf{q}',t)\rangle \;=\; 2\pi^2a^2v_0^2\frac{D_r(Gq^2+D_r)+\Omega^2}{\left(Gq^2+D_r\right)^2+\Omega^2}\delta(\mathbf{q}+\mathbf{q}')\;. \tag{S.48}$$

Finally, the equal-time continuous Fourier velocity correlation components can be expressed as

$$\langle \tilde{v}_{\rm L}(\mathbf{q},t)\tilde{v}_{\rm L}(\mathbf{q}',t)\rangle \;=\; 2\pi^2a^2v_0^2\frac{1+\chi(\xi_{\rm L}q)^2}{1+2\chi(\xi_{\rm L}q)^2+(\xi_{\rm L}q)^4}\delta(\mathbf{q}+\mathbf{q}')\;, \tag{S.49}$$

$$\langle \tilde{v}_{\rm T}(\mathbf{q},t)\tilde{v}_{\rm T}(\mathbf{q}',t)\rangle \;=\; 2\pi^2a^2v_0^2\frac{1+\chi(\xi_{\rm T}q)^2}{1+2\chi(\xi_{\rm T}q)^2+(\xi_{\rm T}q)^4}\delta(\mathbf{q}+\mathbf{q}')\;, \tag{S.50}$$

where the longitudinal and transverse characteristic length scales are respectively

$$\xi_{\rm L}=\sqrt{\frac{B+G}{\sqrt{D_r^2+\Omega^2}}}\quad,\quad \xi_{\rm T}=\sqrt{\frac{G}{\sqrt{D_r^2+\Omega^2}}}, \tag{S.51}$$

and the control parameter is $\chi = D_r/\sqrt{D_r^2+\Omega^2}$.

The final equal-time continuous Fourier velocity correlation expression if therefore

$$\langle \tilde{\mathbf{v}}(\mathbf{q},t)\cdot\tilde{\mathbf{v}}(\mathbf{q}',t)\rangle \;=\; 2\pi^2a^2v_0^2\left[\frac{1+\chi(\xi_{\rm L}q)^2}{1+2\chi(\xi_{\rm L}q)^2+(\xi_{\rm L}q)^4}+\frac{1+\chi(\xi_{\rm T}q)^2}{1+2\chi(\xi_{\rm T}q)^2+(\xi_{\rm T}q)^4}\right]\delta(\mathbf{q}+\mathbf{q}')\;. \tag{S.52}$$

It is important to emphasize that Eq. (S.52) was obtained in the continuum formulation, where $\delta(\mathbf{q}+\mathbf{q}')$ is a Dirac delta distribution. Hence, $\langle \tilde{\mathbf{v}}(\mathbf{q},t)\cdot\tilde{\mathbf{v}}(\mathbf{q}',t)\rangle$ is infinite if one sets $\mathbf{q}'=-\mathbf{q}$. To compare with numerical results, one has to come back to the discrete formulation, corresponding to a finite system size L. The Dirac delta is then replaced by Kronecker delta, according to the substitution rule. One also needs to replace the continuum Fourier transform $\tilde{\mathbf{v}}(\mathbf{q},t)$ with the discrete one, $\mathbf{v}(\mathbf{q},t)$, according to $\tilde{\mathbf{v}}(\mathbf{q},t)=a^2\mathbf{v}(\mathbf{q},t)$, then using $N=L^2/a^2$ we thus end up with

$$\langle \mathbf{v}(\mathbf{q},t)\cdot\mathbf{v}(-\mathbf{q},t)\rangle = \frac{Nv_0^2}{2}\left[\frac{1+\chi(\xi_{\rm L}q)^2}{1+2\chi(\xi_{\rm L}q)^2+(\xi_{\rm L}q)^4}+\frac{1+\chi(\xi_{\rm T}q)^2}{1+2\chi(\xi_{\rm T}q)^2+(\xi_{\rm T}q)^4}\right]\;. \tag{S.53}$$

1. Active Brownian Particles(ABPs): In the absence of chirality ($\Omega=0$), the longitudinal and transverse characteristic length scales become $\xi_{\rm L}=\sqrt{(B+G)/D_r}$, $\xi_{\rm T}=\sqrt{G/D_r}$. Thus, the equal-time continuous velocity correlations simplify to the active Brownian disks solution [S1]

$$\langle \mathbf{v}(\mathbf{q},t)\cdot\mathbf{v}(-\mathbf{q},t)\rangle = \frac{Nv_0^2}{2}\left[\frac{1}{1+(\xi_{\rm L}q)^2}+\frac{1}{1+(\xi_{\rm T}q)^2}\right]\;. \tag{S.54}$$

2. Chiral Active Particles(CAPs): In the absence of rotational noise ($D_r=0$), the longitudinal and transverse characteristic length scale becomes $\xi_{\rm L}=\sqrt{(B+G)/\Omega}$, $\xi_{\rm T}=\sqrt{G/\Omega}$. The equal-time continuous velocity correlation thus simplified to

$$\langle \mathbf{v}(\mathbf{q},t)\cdot\mathbf{v}(-\mathbf{q},t)\rangle = \frac{Nv_0^2}{2}\left[\frac{1}{1+(\xi_{\rm L}q)^4}+\frac{1}{1+(\xi_{\rm T}q)^4}\right]\;. \tag{S.55}$$

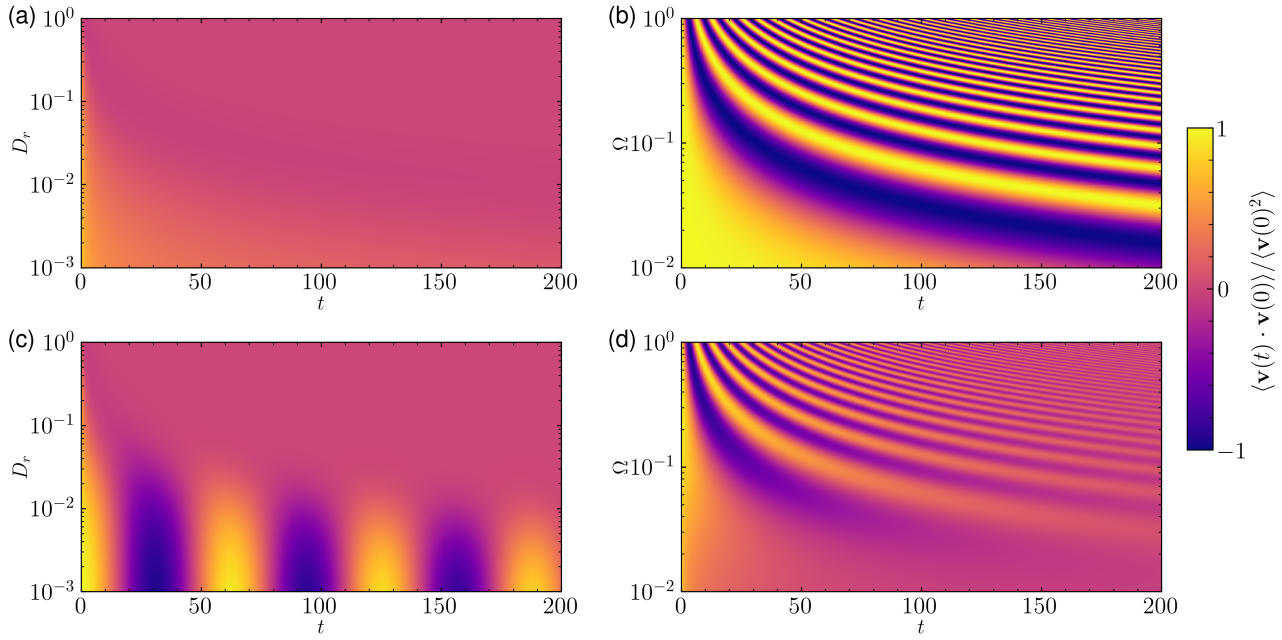

FIG. S.3. Visualization of the normalized velocity autocorrelation function $\langle \mathbf{v}(t)\cdot\mathbf{v}(0)\rangle/\langle \mathbf{v}(0)^2\rangle$, given by Eq. (S.63), as a function of time t and of the rotational diffusion D_r or the chirality Ω. Panels (a) and (b) show the limiting cases: (a) active Brownian disks ($\Omega = 0$) and (b) noiseless chiral active disks ($D_r = 0$). Figures (c) and (d) show intermediate cases with (c) different D_r for constant $\Omega = 0.1$ and (d) different Ω for constant $D_r = 0.01$.

B. Mean-squared velocity

We calculate here the real-space mean-squared velocity $\langle|\mathbf{v}(\mathbf{r},t)|^2\rangle$. First, we have

$$\langle \mathbf{v}(\mathbf{r},t)\cdot\mathbf{v}(\mathbf{r},t)\rangle \;=\; \frac{1}{(2\pi)^4}\int d^2\mathbf{q}\int d^2\mathbf{q}'\;\langle \tilde{\mathbf{v}}(\mathbf{q},t)\cdot\tilde{\mathbf{v}}(\mathbf{q}',t)\rangle\;\mathrm{e}^{-\mathrm{i}(\mathbf{q}+\mathbf{q}')\cdot\mathbf{r}}\;. \tag{S.56}$$

Using equation (S.53), we obtain

$$\langle \mathbf{v}(\mathbf{r},t)\cdot\mathbf{v}(\mathbf{r},t)\rangle \;=\; \frac{a^2v_0^2}{8\pi^2}\int d^2\mathbf{q}\left[\frac{1+\chi(\xi_\mathrm{L}q)^2}{1+2\chi(\xi_\mathrm{L}q)^2+(\xi_\mathrm{L}q)^4}+\frac{1+\chi(\xi_\mathrm{T}q)^2}{1+2\chi(\xi_\mathrm{T}q)^2+(\xi_\mathrm{T}q)^4}\right]\;. \tag{S.57}$$

The physical upper limit of this integral is set by the inverse particle size, i.e., by $q_m = 2\pi/a$. Therefore, using $\int d^2q = 2\pi\int qdq = \pi\int d(q^2)$, we can compute

$$\langle|\mathbf{v}|^2\rangle \;=\; \frac{a^2v_0^2}{4\pi}\int dq\;q\left[\frac{1+\chi(\xi_\mathrm{L}q)^2}{1+2\chi(\xi_\mathrm{L}q)^2+(\xi_\mathrm{L}q)^4}+\frac{1+\chi(\xi_\mathrm{T}q)^2}{1+2\chi(\xi_\mathrm{T}q)^2+(\xi_\mathrm{T}q)^4}\right]\;. \tag{S.58}$$

We can solve the integration numerically to obtain the mean-squared velocity. We can also get the closed-form analytic solution in limiting cases. For $\Omega = 0$, the closed-form mean-squared velocity solution of ABPs will be [S1]

$$\langle|\mathbf{v}|^2\rangle \;=\; \frac{v_0^2}{8\pi}\left[\frac{a^2}{\xi_\mathrm{L}^2}\log(1+\xi_\mathrm{L}^2q_m^2)+\frac{a^2}{\xi_\mathrm{T}^2}\log(1+\xi_\mathrm{T}^2q_m^2)\right]\;. \tag{S.59}$$

In the absence of rotational noise ($D_r = 0$), we instead get the mean-squared velocity for CAPs, given by

$$\langle|\mathbf{v}|^2\rangle \;=\; \frac{v_0^2}{8\pi}\left[\frac{a^2}{\xi_\mathrm{L}^2}\tan^{-1}(\xi_\mathrm{L}^2q_m^2)+\frac{a^2}{\xi_\mathrm{T}^2}\tan^{-1}(\xi_\mathrm{T}^2q_m^2)\right]\;. \tag{S.60}$$

C. Velocity autocorrelation function

We compute the velocity autocorrelation function

$$\langle \mathbf{v}(t)\cdot\mathbf{v}(t')\rangle \;=\; \frac{1}{(2\pi)^4}\int d^2\mathbf{q}\int d^2\mathbf{q}'\;\langle \tilde{\mathbf{v}}(\mathbf{q},t)\cdot\tilde{\mathbf{v}}(\mathbf{q}',t')\rangle\;. \tag{S.61}$$

We write $\langle \tilde{\mathbf{v}}(\mathbf{q},t)\cdot\tilde{\mathbf{v}}(\mathbf{q}',t')\rangle$ as an integral over inverse time ω,ω',

$$\langle \tilde{\mathbf{v}}(\mathbf{q},t)\cdot\tilde{\mathbf{v}}(\mathbf{q}',t')\rangle = \frac{1}{(2\pi)^2}\int_{-\infty}^{\infty} d\omega \int_{-\infty}^{\infty} d\omega' \mathrm{e}^{-\mathrm{i}(\omega t+\omega' t')}\langle \tilde{\mathbf{v}}(\mathbf{q},\omega)\cdot\tilde{\mathbf{v}}(\mathbf{q}',\omega')\rangle \ , \tag{S.62}$$

where $\langle \tilde{\mathbf{v}}(\mathbf{q},\omega)\cdot\tilde{\mathbf{v}}(\mathbf{q}',\omega')\rangle$ was already calculated in III A. Finally, using $\int d^2q = 2\pi\int qdq$, the velocity autocorrelation becomes

$$\begin{aligned}\langle \mathbf{v}(t)\cdot\mathbf{v}(0)\rangle &= \frac{a^2v_0^2}{4\pi}\int_0^{q_m} dq\ q\ \Bigg[\frac{\left[\left[(B+G)^2q^4(\Omega^2-D_r^2)+(\Omega^2+D_r^2)^2\right]\cos(\Omega\ t)-2\Omega D_r(B+G)^2q^4\sin(\Omega\ t)\right]\mathrm{e}^{-D_rt}}{[((B+G)^2q^4+\Omega^2-D_r^2)^2+4D_r^2\Omega^2]}\\ &+ \frac{\left[\left[G^2q^4(\Omega^2-D_r^2)+(\Omega^2+D_r^2)^2\right]\cos(\Omega\ t)-2\Omega D_rG^2q^4\sin(\Omega\ t)\right]\mathrm{e}^{-D_rt}}{[(G^2q^4+\Omega^2-D_r^2)^2+4D_r^2\Omega^2]}\\ &- \frac{(B+G)q^2D_r(D_r^2+\Omega^2-(B+G)^2q^4)\mathrm{e}^{-(B+G)q^2t}}{[(D_r^2+\Omega^2-(B+G)^2q^4)^2+4(B+G)^2q^4\Omega^2]} - \frac{Gq^2D_r(D_r^2+\Omega^2-G^2q^4)\mathrm{e}^{-Gq^2t}}{[(D_r^2+\Omega^2-G^2q^4)^2+4G^2q^4\Omega^2]}\Bigg]\end{aligned} \tag{S.63}$$

In Fig. S.3, we illustrate the normalized velocity autocorrelation functions, $\langle \mathbf{v}(t)\cdot\mathbf{v}(0)\rangle/\langle \mathbf{v}(0)^2\rangle$, as a function of time t, in accordance with the equation detailed in the velocity autocorrelation continuum Eq. (S.63).

In Fig. S.3(a), the velocity autocorrelation for ABPs ($\Omega = 0$) is depicted, highlighting the persistent decay of the autocorrelation with a small rotational diffusion coefficient D_r. In Fig. S.3(b), we plot the velocity autocorrelation for CAPs ($D_r = 0$), which demonstrates the sustained oscillatory behavior of the velocity autocorrelation.

We plot the velocity autocorrelation functions for CABPs in Fig. S.3(c) with varying D_r for constant Ω and in Fig. S.3(d) with varying Ω for constant D_r. We observe decaying oscillatory behavior for low rotational diffusion constant $D_r \leq \Omega$ in Fig. S.3(c) and for high chirality $\Omega \geq D_r$ values in Fig. S.3(d).

IV. HETEROGENEOUS MIXTURES

A. Binary mixtures

We consider the binary mixtures of two species A and B with packing fractions ϕ_A and ϕ_B respectively with total packing fractions ϕ. Spatial velocity autocorrelation in Fourier space reads :

$$\langle \mathbf{v}(\mathbf{q},t)\cdot\mathbf{v}(-\mathbf{q},t)\rangle = \frac{\phi_A}{\phi}\langle \mathbf{v}(\mathbf{q},t)\cdot\mathbf{v}(-\mathbf{q},t)\rangle_A + \frac{(\phi-\phi_A)}{\phi}\langle \mathbf{v}(\mathbf{q},t)\cdot\mathbf{v}(-\mathbf{q},t)\rangle_B \ . \tag{S.64}$$

Now, the velocity autocorrelation also reads :

$$\langle \mathbf{v}(t)\cdot\mathbf{v}(0)\rangle = \frac{\phi_A}{\phi}\langle \mathbf{v}(t)\cdot\mathbf{v}(0)\rangle_A + \frac{(\phi-\phi_A)}{\phi}\langle \mathbf{v}(t)\cdot\mathbf{v}(0)\rangle_B \ . \tag{S.65}$$

In Fig. S.4, we plot the color map of the velocity autocorrelation functions given by Eq. (S.65) for binary mixtures, characterized by the relative packing fraction of A, defined by ϕ_A/ϕ.

In Fig. S.4(a), we depict the binary mixtures of CABPs(Species-A) and ABPs(Species-B). The two limiting uniform cases are: ABPs for $\phi_A/\phi = 0$ and CABPs for $\phi_A/\phi = 1$. As we increase the fraction of Species-A ϕ_A/ϕ leads to oscillation with a time period $T = 2\pi/\Omega = 20\pi$.

In Fig. S.4(b), we present the binary mixtures of CABPs with two different chiralities: Species-A with $\Omega = 0.1$ and Species-B with $\Omega = 0.2$. The two limiting uniform cases are: for $\phi_A/\phi = 0$, CABPs with chirality $\Omega = 0.2$ set time period $T = 10\pi$; and for $\phi_A/\phi = 1$, CABPs with chirality $\Omega = 0.1$ set time period $T = 20\pi$. We observe the dominance of two chiralities in the intermediate packing fractions around $\phi_A/\phi \sim 0.5$.

In Fig. S.4(c), we present the binary mixtures of CABPs with two different rotational diffusion constants: Species-A with $D_r = 0.01$ and Species-B with $D_r = 0.1$. The two limiting uniform cases are: CABPs (Species-B with $D_r = 0.1$) for $\phi_A/\phi = 0$ and CABPs (Species-A with $D_r = 0.01$) for $\phi_A/\phi = 1$. We can clearly see the dominance of oscillatory behavior as the fraction of particles with a high rotational diffusion coefficient (Species-B) decreases.

We compare the analytical velocity autocorrelation functions of the three types of binary mixtures discussed here with $\phi_A/\phi = 0.5$ to their corresponding simulations, as shown in Fig. 6(a) of the main article.

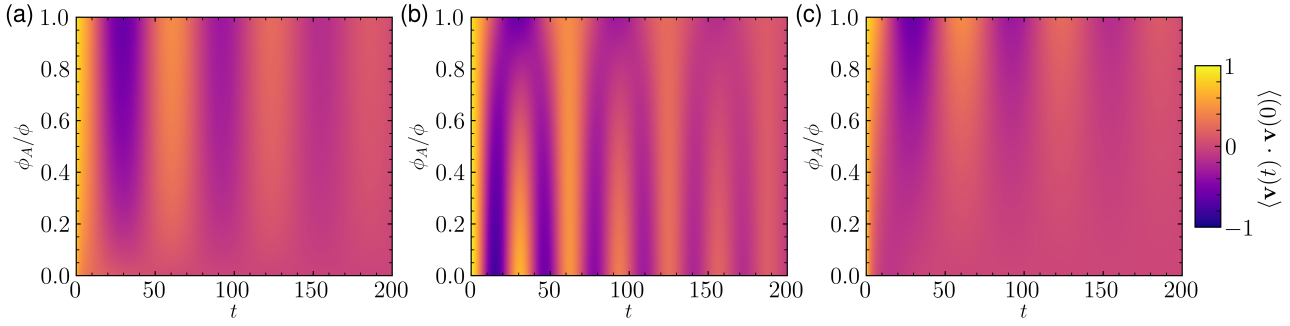

FIG. S.4. Visualization of the normalized velocity autocorrelation function $\langle \mathbf{v}(t)\cdot\mathbf{v}(0)\rangle/\langle \mathbf{v}(0)^2\rangle$ as a function of time t for binary mixtures of active disks, obtained through the continuum elastic formulation. Panel (a) represents binary mixtures of Species A (chiral active Brownian disks with $\Omega = 0.1$ and packing fraction ϕ_A) and Species B (non chiral active Brownian disks with $\Omega = 0$ and packing fraction $\phi - \phi_A$). Panel (b) shows binary mixtures of Species A (chiral active Brownian disks with $\Omega = 0.1$ and packing fraction ϕ_A) and Species B (chiral active Brownian disks with $\Omega = 0.2$ and packing fraction $\phi - \phi_A$). Both species in (a) and (b) have rotational diffusion coefficient $D_r = 0.01$. Panel (c) illustrates binary mixtures of Species A (chiral active Brownian disks with $D_r = 0.01$ and packing fraction ϕ_A) and Species B (chiral active Brownian disks with $D_r = 0.1$ and packing fraction $\phi - \phi_A$). Both species in (c) have chirality $\Omega = 0.1$.

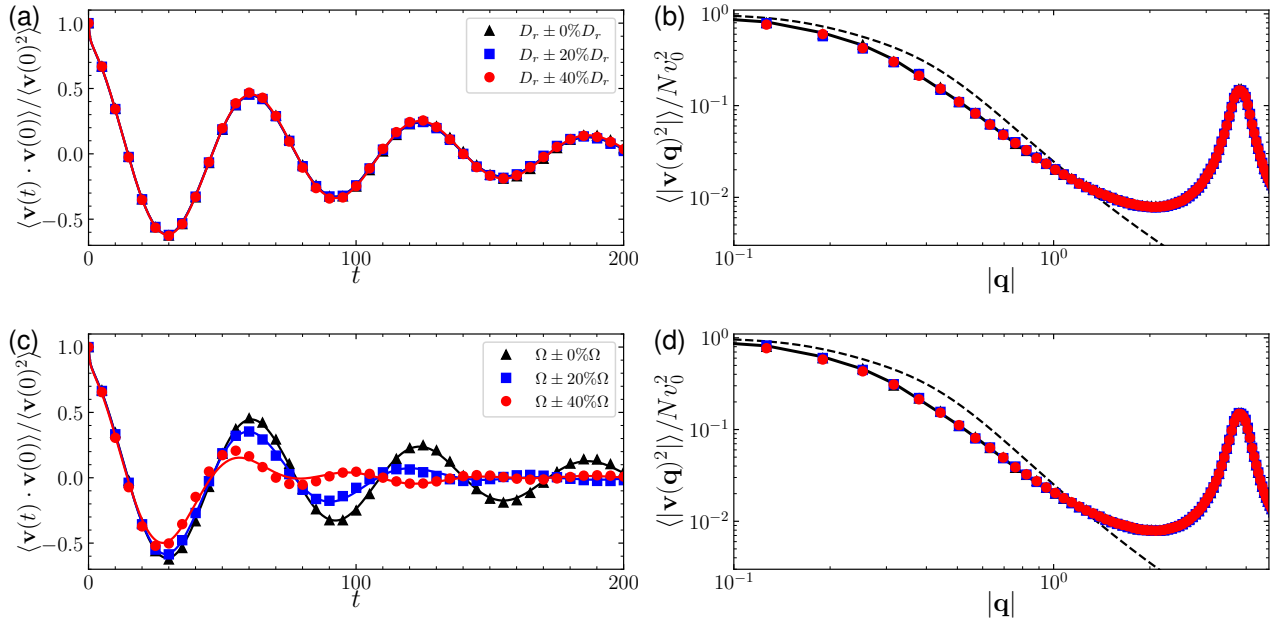

FIG. S.5. Effects of heterogeneity in chiral active solids. (a) Normalized velocity autocorrelation function defined by $\langle \mathbf{v}(t)\cdot\mathbf{v}(0)\rangle/\langle \mathbf{v}(0)^2\rangle$. Points are simulation results. The solid lines result from the continuum elastic formulation. (b) Spatial velocity correlation functions in Fourier space defined by $\langle |\mathbf{v}(\mathbf{q})|^2\rangle/Nv_0^2$. The dashed and solid lines result from the continuum elastic formulation and the normal mode formulation, respectively. We consider complex mixtures of particles with constant chirality $\Omega = 0.1$ and a mean rotational diffusion coefficient $D_r = 0.01$ with a uniform distribution spanning $\pm 20\%$ and $\pm 40\%$ of the mean. (c) Normalized velocity autocorrelation function. Points are simulation results. The solid lines result from the continuum elastic formulation. (d) Spatial velocity correlation functions in Fourier space. The dashed and solid lines results from the continuum elastic formulation and the normal mode formulation, respectively. We consider complex mixtures of particles with constant rotational diffusion coefficient $D_r = 0.01$ and a mean chirality $\Omega = 0.1$ with a uniform distribution spanning $\pm 20\%$ and $\pm 40\%$ of the mean.

B. Complex mixtures

We can extend the superposition results of binary mixtures to the complex situations, for n-component systems with packing fractions $\phi_1, \phi_2, ..., \phi_n$ and total packing fraction $\phi = \sum_{i=1}^{n} \phi_i$. We can thus write the spatial velocity

correlation in Fourier space as

$$\langle \mathbf{v}(\mathbf{q},t)\cdot\mathbf{v}(-\mathbf{q},t)\rangle \;=\; \frac{\sum_{i=1}^{n}\phi_i\langle \mathbf{v}(\mathbf{q},t)\cdot\mathbf{v}(-\mathbf{q},t)\rangle_i}{\sum_{i=1}^{n}\phi_i}\;. \tag{S.66}$$

And the velocity autocorrelation as

$$\langle \mathbf{v}(t)\cdot\mathbf{v}(0)\rangle \;=\; \frac{\sum_{i=1}^{n}\phi_i\langle \mathbf{v}(t)\cdot\mathbf{v}(0)\rangle_i}{\sum_{i=1}^{n}\phi_i}\;. \tag{S.67}$$

We utilize Eq. (S.66) and Eq. (S.67) to compute the spatial velocity correlation in Fourier space $\langle \mathbf{v}(\mathbf{q},t)\cdot\mathbf{v}(-\mathbf{q},t)\rangle$ and the velocity autocorrelation functions $\langle \mathbf{v}(t)\cdot\mathbf{v}(0)\rangle$, respectively for a chiral active solid composed of n-component complex mixtures.

We consider the complex mixtures of CABPs with uniform variations in the rotational diffusion coefficients D_r, as illustrated in Figs. S.5(a,b) and with uniform variations in the chirality Ω, as shown in Figs. S.5(c,d). Remarkably, the velocity autocorrelation functions in Fig. S.5(a) and spatial velocity correlations in Fourier space in Fig. S.5(b) both remain invariant with uniform variations in rotational diffusion coefficient D_r. Additionally, the velocity autocorrelation functions in Fig. S.5(c) are suppressed and spatial velocity correlations in Fourier space in Fig. S.5(d) remain invariant with uniform variations in chirality Ω.

This suggests that variations in D_r do not impact the velocity autocorrelation functions while variations in Ω do impact these functions. The spatial velocity correlations in Fourier space remain invariant under both conditions, even with variations up to 40% (see Fig. 6(d) in the main article).

[S1] S. Henkes, K. Kostanjevec, J. M. Collinson, R. Sknepnek, and E. Bertin, Dense active matter model of motion patterns in confluent cell monolayers, Nature Communications **11**, 1405 (2020).

[S2] P. M. Chaikin and T. C. Lubensky, *Principles of Condensed Matter Physics* (Cambridge University Press, Cambridge, 1995).